*7316–7328* *Nucleic Acids Research, 2011, Vol. 39, No. 16* *Published online 27 May 2011*
*doi:10.1093/nar/gkr271*

# The biological and structural characterization of *Mycobacterium tuberculosis* UvrA provides novel insights into its mechanism of action

**Franca Rossi[1], Jasbeer Singh Khanduja[2], Alessio Bortoluzzi[1], Joanna Houghton[3], Peter Sander[4], Carolin Güthlein[4], Elaine O. Davis[3], Burkhard Springer[5], Erik C. Böttger[4], Annalisa Relini[6], Amanda Penco[6], K. Muniyappa[2] and Menico Rizzi[1,*]**

[1]DiSCAFF, University of Piemonte Orientale 'Amedeo Avogadro', Via Bovio 6, 28100 Novara, Italy, [2]Department of Biochemistry, Indian Institute of Science, Bangalore 560 012, India, [3]Division of Mycobacterial Research, MRC National Institute for Medical Research, The Ridgeway Mill Hill, London, UK, [4]Institut für Medizinische Mikrobiologie, University of Zürich, Gloriastrasse 30/32, CH-8006 Zürich, Switzerland, [5]Institut für Medizinische Mikrobiologie und Hygiene, Universitätsplatz 4, 8010 Graz, Austria and [6]Department of Physics, University of Genoa, Via Dodecaneso, 33, 16146 Genoa, Italy

Received September 13, 2010; Revised March 17, 2011; Accepted April 4, 2011

## ABSTRACT

***Mycobacterium tuberculosis* is an extremely well adapted intracellular human pathogen that is exposed to multiple DNA damaging chemical assaults originating from the host defence mechanisms. As a consequence, this bacterium is thought to possess highly efficient DNA repair machineries, the nucleotide excision repair (NER) system amongst these. Although NER is of central importance to DNA repair in *M. tuberculosis*, our understanding of the processes in this species is limited. The conserved UvrABC endonuclease represents the multi-enzymatic core in bacterial NER, where the UvrA ATPase provides the DNA lesion-sensing function. The herein reported genetic analysis demonstrates that *M. tuberculosis* UvrA is important for the repair of nitrosative and oxidative DNA damage. Moreover, our biochemical and structural characterization of recombinant *M. tuberculosis* UvrA contributes new insights into its mechanism of action. In particular, the structural investigation reveals an unprecedented conformation of the UvrB-binding domain that we propose to be of functional relevance. Taken together, our data suggest UvrA as a potential target for the development of novel anti-tubercular agents and provide a biochemical framework for the identification of small-molecule inhibitors interfering with the NER activity in *M. tuberculosis*.**

## INTRODUCTION

During its life, *Mycobacterium tuberculosis* is exposed to numerous genotoxic insults originating from both antimicrobial host defence mechanisms and the environment (1). Since persistence within the infected macrophage and reactivation of the bacillus from the dormant state are key features of infection, the maintenance of genome integrity is considered a vital aspect in the biology of *M. tuberculosis* (2,3).

One of the major molecular machines that control chromosome stability in living species is represented by the nucleotide excision repair (NER) system (4–7) that is capable of repairing a wide variety of DNA lesions (reviewed in ref. 5). In Eubacteria and some Archaea, the first steps in NER are carried out by UvrA, UvrB and UvrC proteins, often referred to as the UvrABC endonuclease. This multi-enzymatic complex recognizes the damage and excises a short lesion-containing DNA oligonucleotide, in a multi-step process in which the three proteins act in concert. Briefly, an UvrA•B heteromeric complex scans the DNA searching for damaged sites. The identity of the UvrA•B oligomeric state and of the searching complex have long been the subject of debate and controversy; however, two independent studies using fluorescence resonance energy

*To whom correspondence should be addressed. Tel: +39 0321 375 712; Fax: +39 0321 375 821; Email: rizzi@pharm.unipmn.it

The authors wish it to be known that, in their opinion, the first two authors should be regarded as joint First Authors.

transfer and single-molecule imaging of quantum-dot-labelled proteins have proposed that the ATP-bound $UvrA_2$•$B_2$ complex is the stable form that slides along the DNA until a damaged site is encountered (8,9). Once recognized by the UvrA component, the injured strand is transferred to UvrB and UvrA is released. UvrC is then recruited at the UvrB•DNA complex where it performs a single strand incision on both sides of the damaged site. Subsequently, the helicase UvrD removes the excised oligonucleotide and DNA polymerase I fills the gap, using the intact complementary strand as the template. Finally, DNA ligase seals the nick, thus restoring the integrity of the double helix (5).

Information is beginning to emerge concerning the role of NER in the biology of mycobacteria, an observation that assumes even more emphasis considering that these bacteria lack a functional DNA mismatch repair system (2). Transcription of the *uvr*A gene has been shown to be up-regulated in human macrophage-grown *M. tuberculosis bacilli* hours post-infection (10). Gene inactivation and trans-complementation analyses demonstrated a crucial role for UvrB in mycobacterial resistance to nitrosative, oxidative and UV exposure-induced DNA damage (11–13), as well as the importance of the gene for *M. tuberculosis* survival and virulence in the mouse model (12). Only very recently experimental evidences supporting the cooperativity of the enzymatic actions of *M. tuberculosis* UvrA, UvrB and UvrC and their participation in mycobacterial NER has been provided (14).

In bacteria, UvrA performs the ATP-dependent, lesion-sensing activity that initiates the highly ordered recruitment of NER components to the damaged site (5,6). Sequence comparison analyses allowed the assignment of UvrA to the ATP binding cassette (ABC) ATPase superfamily (Pfam code: PF09818), whose members are involved in many different cellular functions, ranging from import/export transport across the membranes to non-transport-related phenomena, DNA repair among these (15).

To date, three crystal structures of UvrA members are present in the Protein Data Bank, and they correspond to the class I UvrA from *Bacillus sthearothermophilus* in complex with ADP (*Bst*UvrA•ADP) (16), the functional orthologue from *Thermotoga maritima* associated to modified DNA (*Tm*UvrA•DNA) (17) and the class II UvrA from *Deinococcus radiodurans* (*Dr*UvrA2) (18). These structural investigations disclosed the multi-domain molecular architecture of UvrA, which is characterized by conserved nucleotide binding domains (NBD), where ATP hydrolysis takes place (5,6,19), and by unique domains, namely the UvrB binding domain (UvrB-BD), which is peculiarly absent in class II UvrAs (*Dr*UvrA2 among these) and the insertion domain (ID), distinguishing UvrAs from other ABC ATPases. Structural and biochemical investigations focusing on the UvrA-DNA and UvrA-UvrB interaction have also been carried out (17,20–22), contributing to deciphering the dynamics of the first steps in NER of a small number of bacterial species. In contrast, since little is known of the *M. tuberculosis* UvrABC endonuclease our understanding of NER in this important human pathogen is still limited.

We report here an integrated analysis of *M. tuberculosis* UvrA. Our data indicate a key functional role for UvrA in protection against reactive oxygen and nitrogen species-triggered DNA damage. Moreover, we show that the DNA binding activity of *M. tuberculosis* UvrA towards various DNA structures mimicking intermediates of DNA repair, is correlated to the amount of single-stranded regions within the DNA substrate and provide evidence that the low intrinsic ATPase activity of *M. tuberculosis* UvrA is markedly stimulated by DNA. Finally, the crystal structure determination of *M. tuberculosis* UvrA in its ligand-free form reveals a remarkable repositioning of the UvrB binding domain and could therefore represent a further insight in the very initial steps of UvrABC complex assembling at the site of DNA lesion.

## MATERIALS AND METHODS

### Functional characterization of *M. tuberculosis uvrA* mutant strain

*Bacterial strains, media and culture conditions*. Standard procedures were adopted for cloning and propagation of plasmids in *Escherichia coli*. The *M. tuberculosis* wild-type strain used was 1424, a derivative of *M. tuberculosis* H37Rv carrying a non-restrictive *rpsL* mutation conferring streptomycin resistance (23). The *M. tuberculosis uvrB* mutant strain MHD9 (11,12) was kindly provided by H. Darwin and C. Nathan. Cultures of *M. tuberculosis* were grown in OADC enriched Middlebrook 7H9 medium or modified Dubos (Difco) supplemented with albumin and 0.2% glycerol at 37°C in a rolling incubator at 2 rpm. When appropriate, antibiotics were added at the following concentrations: kanamycin 50 μg/ml; streptomycin 100 μg/ml; gentamicin 5 μg/ml. All procedures with *M. tuberculosis* were carried out under Containment level 3 conditions.

*Isolation of a M. tuberculosis* uvrA *mutant strain and gene complementation analysis*. Allelic replacement techniques (24) were used to generate an *M. tuberculosis* knockout mutant for *uvrA* (*Rv1638*). A 5.9 kb NotI fragment containing the *uvrA* gene was isolated from BAC *Rv401* (25) and cloned into pBluescript KS(-) (Stratagene) previously digested with NotI to result in pBluescript-*uvrA*. For functional inactivation of *uvrA* the plasmid was digested with EcoNI and StuI (deleting 1340 bp) and a 1.2 kb fragment containing the kanamycin resistance cassette from plasmid pUC4K (GE Healthcare) was inserted to result in plasmid p*uvrA::aph*. From this plasmid a 5.9 kb NotI fragment containing the inactivated *uvrA* gene (lacking base pairs 924–2263 of the 2919 bp *uvrA* ORF) was subcloned into plasmid pBluescript-*rpsL* (M.s.) previously digested with NotI resulting in plasmid p*uvrA::aph-rpsL*. pBluescript-*rpsL* (M.s.) is a derivative of pBluescript carrying a 0.9 kb fragment with the *rpsL* gene of *M. smegmatis*. To isolate a mutant strain, the targeting construct was transformed into the streptomycin-resistant *M. tuberculosis* strain 1424, plating on medium-containing kanamycin to select for chromosomal integration of the knockout plasmid. Following the identification of transformants

that had undergone a homologous single crossover by Southern blot analyses, counter selection on streptomycin in the presence of kanamycin was used to obtain colonies arising from a double crossover event. Southern analyses were performed to identify mutant strains using a 628 bp 3′-probe (NcoI/NotI) with BamHI-digested DNA (Supplementary Figure S1).

For complementation, a 3694 bp fragment of DNA including the entire coding sequence of *uvrA* and 383 bp of the upstream region was cloned into the HindIII site of the integrating plasmid pKP203, resulting in pJH08. This vector is equivalent to pKP186 (26) but has a fragment conferring gentamycin resistance in place of the kanamycin resistance gene (K.G. Papavinasasundaram, personal communication). As these plasmids lack the integrase gene, pJH08 was co-transformed into the *uvrA* mutant strain with pBS-Int (27), which is a suicide plasmid that supplies the integrase function but is subsequently lost from the cells.

*Susceptibility to DNA damaging agents*. To assess the susceptibilities of the strains to UV irradiation, cultures were grown rolling to $A_{600}$ of 0.3–0.4 and 10-fold serial dilutions were prepared in PBS/0.05% Tween-80. Ten microlitres of each dilution were spread on quarter plates of four-sector plates (BD-Falcon), in duplicate for each dose to be used. Plates with lids removed were then exposed to UV irradiation at 254 nm for various times to give doses ranging from 0 to 33 $J \bullet m^{-2}$. The plates were then incubated in the dark until colonies were visible and CFU enumerated.

For *in vitro* survival experiments following exposure to mitomycin C (0.2 μg/ml), *t*-butyl hydroperoxide (0.1 mM) or sodium nitrite pH 5.5 (2 mM), cultures were grown rolling to late exponential phase ($A_{600}$ = 0.8–1.0) and survival was determined as described (12) with the following modifications. Acidified medium (pH 5.5) was used for the nitrite stress and its pH control only; for the other stresses standard medium was used (pH 7.2). Triplicate 190 μl samples of diluted cell suspensions were incubated with 10 μl stress agent (or medium as control) for 6 days, except for mitomycin C where incubation was for 24 h. Serial dilutions were prepared and plated in triplicate for CFU determination.

In each case, three independent biological replicates were performed. Survival was calculated by the ratio of CFU of the treated cultures compared to the CFU of the untreated controls.

### Recombinant *Mt*UvrA expression, purification and biochemical characterization

*Subcloning*. In order to obtain the p*Mt*HisUvrA expression construct, the *uvrA* ORF of *Mycobacterium tuberculosis* H37Rv (Tuberculist entry: Rv1638) was amplified by PCR using 20 ng of MTCY06H11.01 bacmid DNA (Institut Pasteur, Paris, France) and subcloned into the pET16b vector (Novagen), adopting standard recombinant DNA procedures (28), as detailed in 'Supplementary Data'. The resulting plasmid drives in *E. coli* the IPTG-inducible synthesis of a N-terminally His-tagged *Mt*UvrA (predicted molecular mass of 108 652.1 Da; 993 amino acid residues) (Supplementary Figure S2a).

*DNA substrates*. The sequences of oligonucleotides used in this study are listed in Supplementary Table S1. The oligonucleotides (ODN) were labelled at the 5′-end by [γ-$^{32}$P]ATP using T4 polynucleotide kinase (New England Biolabs). DNA substrates were prepared and characterized as described previously (29). Briefly, the $^{32}$P-labelled ODN was annealed to its complementary strand to generate the specified substrate: single-stranded DNA (ODN1*), bubble duplex (ODN2* annealed to ODN3), flayed duplex (ODN1* annealed to ODN4), 5′-flap (ODN1*, ODN4 annealed to ODN5), 5′-overhang (ODN1* annealed to ODN5), non-damaged duplex DNA (ODN1* annealed to ODN6) and damaged duplex DNA (ODN7 annealed to ODN8*). The asterisk represents the ODN containing the radiolabel at the 5′-end. Details of the procedure adopted for generating each substrate is described in 'Supplementary Data'.

*Purification of MtUvrA protein*. *Mycobacterium tuberculosis* UvrA was over-expressed in *E. coli* Rosetta2(DE3) pLysS strain harbouring the plasmid p*Mt*HisUvrA and purified through a two-step chromatographic procedure based on Ni-NTA agarose and heparin-agarose columns. Details for protein over-expression and purification are provided as 'Supplementary Data'.

*Electrophoretic mobility shift assays*. Binding assays (10 μl) contained 50 mM HEPES (pH 7.5), 10 mM $MgCl_2$, 2 mM DTT, 0.25 mM ATPγS, 50 μg/ml BSA, 250 pM of the indicated $^{32}$P-labelled DNA and increasing concentrations of *Mt*UvrA and were carried out as detailed in 'Supplementary Data'.

*ATPase assay*. Reaction mixtures (10 μl) contained 50 mM Tris–HCl (pH 7.5), 10 mM $MgCl_2$, 1 mM DTT, 50 μM [γ-$^{32}$P]ATP, 50 μg/ml BSA, 100 nM DNA substrate as indicated in the figure legends and increasing concentrations of *Mt*UvrA. The reactions and were carried out as detailed in Supplementary Data and the amount of [α-$^{32}$P]ADP in each spot was determined using UVI Band software and plotted as the percent ATP hydrolyzed as a function of increasing concentrations of *Mt*UvrA.

### Crystallographic study

*Crystallization*. The protein used in crystallization trials was prepared by optimizing the purification protocol as reported in 'Supplementary Data'. Optimal crystals were obtained by mixing 1.5 μl of *Mt*UvrA protein solution at 5 mg/ml with an equal volume of a reservoir solution containing 1.5 M ammonium sulphate, 0.1 M HEPES pH 7.0 and 1 mM yttrium chloride. The resulting drop was equilibrated against 500 μl of the reservoir solution, at 20°C.

*Structure determination*. Details of the procedure followed for structure determination and refinement are provided as 'Supplementary Data'. Briefly, diffraction data were collected at 100 K up to 3.4 Å resolution using

**Table 1.** Data collection and refinement statistics

| | *Mt*UvrA |
|---|---|
| Data collection | |
| Space group | $P3_221$ |
| Cell dimensions | |
| *a*, *b*, *c* (Å) | 258.3, 258.3, 204.5 |
| α, β, γ (°) | 90, 90, 120 |
| Resolution (Å) | 93.1–3.4 (3.6–3.4)[a] |
| Observations | 259 797 (37 864) |
| Unique reflections | 106 710 (15 716) |
| $R_{merge}$ | 0.091 (0.40) |
| Multiplicity | 2.4 (2.4) |
| Completeness (%) | 98.9 (100.0) |
| Refinement | |
| No. of protein atoms | 43 673 |
| No. of Zn ions | 14 |
| $R_{work}$ (%) | 25.09 |
| $R_{free}$ (%) | 33.0 |
| R.m.s. deviation bond lengths (Å) | 0.011 |
| R.m.s. deviation bond angles (°) | 1.56 |
| Mean B value (Å$^2$) | 82 |
| Ramachandran plot analysis | |
| Most favoured (%) | 82.3 |
| Additionally allowed (%) | 15.6 |
| Generously allowed (%) | 1.4 |
| Disallowed (%) | 0.7 |

[a]Values in parentheses are for the highest resolution shell.

synchrotron radiation at the BM14 UK beam line (European Synchrotron Radiation Facility, Grenoble, France) and processed with the programmes of the CCP4 suite (30). *Mt*UvrA structure determination was carried out by molecular replacement using the structure of *Bst*UvrA (pdb entry: 2R6F, overall sequence identity between the two orthologues: 51%) (16) as the search model and the program Phaser (31). The initial molecular replacement phases were dramatically improved by a 6-fold density averaging and solvent flattening procedure, as implemented in the programme DM (32). The resulting electron density map allowed the tracing of an almost complete initial model that was subsequently subjected to extensive crystallographic refinement with the program PHENIX (33) alternated with sessions of model building with the program Coot (34). The final model consists of regions: 2-239/248-953 chain A; 2-206/215-235/251-301/313-953 chain B; 2-204/215-234/255-431/437-953 chain C; 2-206/215-240/250-342/347-429/440-953 chain D; 2-122/129-206/215-240/255-343/346-953 chain E; 2-119/307-457/463-702/844-950 chain F. The stereochemistry of the refined model has been assessed with the program PROCHECK (35). Data processing and refinement statistics appear in Table 1. All figures were generated with the program Pymol (36).

The atomic coordinates and structure factors have been deposited with the Protein Data Bank with the accession code 2ygr.

## RESULTS AND DISCUSSION

### Functional analysis of UvrA in *M. tuberculosis*

UvrA plays an important role in the recognition of DNA damage for repair by NER (4,5). To confirm the importance of UvrA in the repair of typical NER substrates and to assess its role in surviving more physiologically relevant DNA damage, a strain of *M. tuberculosis* was constructed in which *uvrA* was inactivated. The *uvrA* mutation consisted of a deletion of 1.34 kb within the 2.92 kb coding sequence and insertion of a kanamycin resistance cassette. The genotype was confirmed by Southern analysis (Supplementary Figure S1). The mutant strain was complemented using an integrating plasmid in which *uvrA* was expressed from its own promoter (see 'Materials and Methods' section).

Typical substrates for repair by NER in other bacteria include intra- and interstrand cross-links, such as those generated by UV irradiation (37) and mitomycin C (38,39), respectively. Therefore, survival of the wild-type, *uvrA* mutant and complemented strains following exposure to these agents was assessed initially, and compared to that previously reported for a *uvrB* mutant (12). As expected the *uvrA* mutant was highly sensitive to UV light, at doses which had only minor effects on the wild-type strain (Figure 1a). The extent of susceptibility of the *uvrA* mutant paralleled that of the *uvrB* mutant, as would be expected since UvrA and UvrB act together in damage recognition (5,14). Complementation of the *uvrA* mutant restored survival to levels similar to those of the wild-type, confirming that the increased susceptibility was due to the inactivation of *uvrA*. Similarly, both the *uvrA* and *uvrB* mutants exhibited enhanced susceptibility to mitomycin C compared with the wild-type and *uvrA*-complemented strains (Figure 1b). These observations confirm the importance of UvrA for NER in *M. tuberculosis* and show that the protein function is non-redundant, i.e. its loss could not be compensated by another mechanism.

Reactive oxygen and nitrogen intermediates represent more physiologically relevant DNA damaging agents (2). Nitrosative and oxidative stress conditions were modelled by exposure to acidified sodium nitrite and *t*-butyl hydroperoxide, respectively (Figure 1c and d), which have been shown previously to cause these types of damage (40,41). The survival of the *uvrA* mutant was reduced compared with the wild-type by exposure to either of these agents. In both cases, the sensitivity of the mutant strain was restored to levels similar to those of the wild-type on complementation. The susceptibility of the *uvrA* mutant to acidified nitrite resembled that observed previously in *M. tuberculosis* when *uvrB* was inactivated (12). However, in contrast to our result, mutation of *uvrB* was reported to not cause increased sensitivity to oxidative stress. This difference may arise from the use of different assays in the two studies: the disk diffusion assay used in the *uvrB* study was probably less sensitive than that used in the present work (CFU determination). It is also possible that the effect seen here is a result of alkylation via the formation of an alkoxy radical (42). Taken together, these data confirm that UvrA is important for the repair of nitrosative and to a lesser extent oxidative DNA damage, and is thus likely to play a role in bacterial survival during infection.

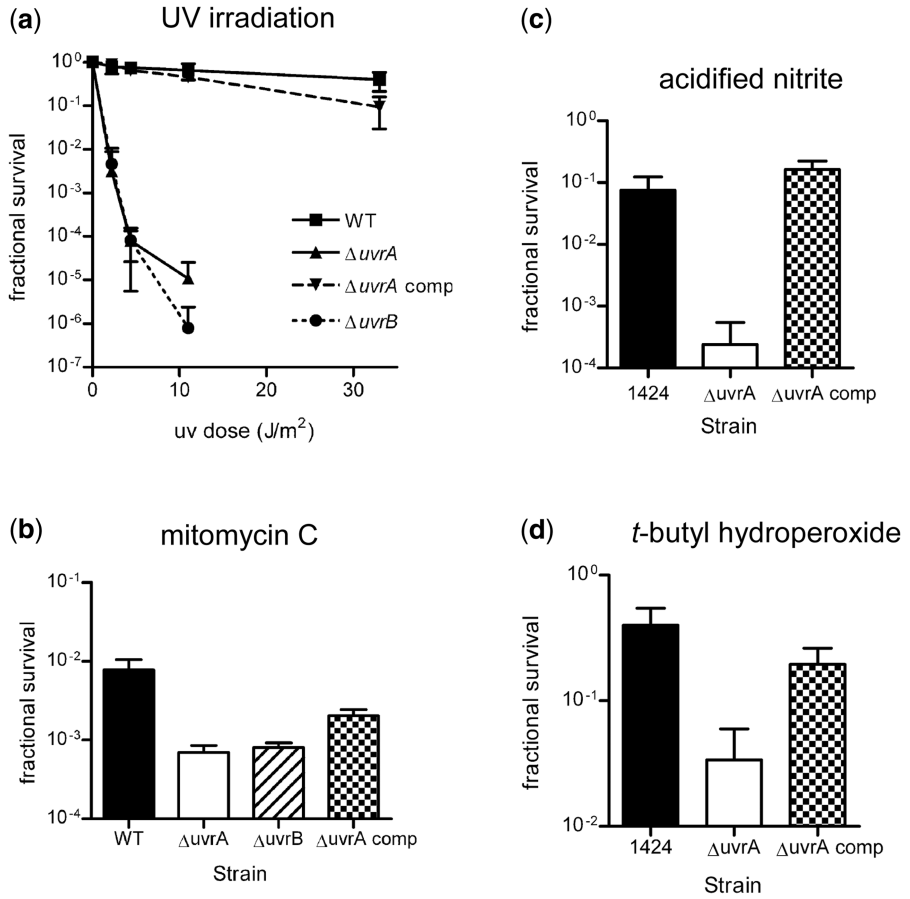


**Figure 1.** Sensitivity of the *uvrA* mutant to genotoxic damage. Survival of the *uvrA* mutant strain (Δ*uvrA*) following exposure to (**a**) UV irradiation, (**b**) mitomycin C, (**c**) reactive nitrogen intermediates and (**d**) reactive oxygen intermediates compared with the wild-type (WT) and complemented (Δ*uvrA* comp) strains upon the same treatment; in each case the surviving fraction was calculated by comparison with an untreated control. In a and b, the survival of an *uvrB* mutant (Δ*uvrB*) upon the same treatment is also shown (see 'Materials and Methods' section). The data shown are the means of duplicate (a) or triplicate (b, c and d) assays from three biological replicates; the error bars represent standard deviations.

### DNA binding activity of *M. tuberculosis* UvrA

The DNA binding activity of purified recombinant *Mt*UvrA was characterized by means of electrophoretic mobility shift assays. Since the sequential two-step mechanism of nucleotide incision begins with the process of damage recognition by UvrA, we used a variety of DNA substrates (Supplementary Table S1) to explore how the local DNA structure influences the binding of the enzyme that ultimately determines the efficiency of the incision. To this end, we used a bona fide NER substrate (43) (i.e. a damaged duplex DNA molecule containing a site-specific lesion represented by a single internal fluoresceinated-dT adduct) and some common intermediates generated during various DNA metabolic processes, such as DNA replication, repair, recombination and transcription. Typically, the assays were performed with 250 pM of the indicated radio-labelled substrate with increasing concentrations of *Mt*UvrA in the presence of 0.25 mM ATPγS and 10 mM $MgCl_2$. The data from electrophoretic mobility shift assays indicate that *Mt*UvrA binds to different DNA structures in the following hierarchical manner: single-stranded DNA > duplex DNA containing a site-specific lesion > bubble duplex > flayed duplex > 5′-flap > 5′-overhang > non-damaged duplex DNA (Figure 2, panels a–g). Quantification of protein–DNA complexes in the respective autoradiograms suggests robust binding of *Mt*UvrA to single stranded and damaged duplex DNA by ~3-fold more efficiently than to the non-damaged duplex DNA (Figure 2, panels h and i). These data are in agreement with the results from *E. coli* UvrA, which displays higher affinity for single-stranded DNA (44). It is noteworthy, however, that *Mt*UvrA has structure-specific DNA binding activity and that the extent of binding correlated with single-stranded DNA within the DNA substrate.

### *Mycobacterium tuberculosis* UvrA displays DNA-dependent ATPase activity

The interaction of UvrA with DNA is regulated by ATP binding and its hydrolysis (5). *Escherichia coli* UvrA was originally characterized as a DNA-independent ATPase (44). However, subsequent studies showed decrease in the $k_M$ and $V_{max}$ for ATP hydrolysis with the addition of increasing concentrations of double-stranded DNA (45). Currently, it is thought that ATP binding is not essential for DNA binding, but ATP hydrolysis is

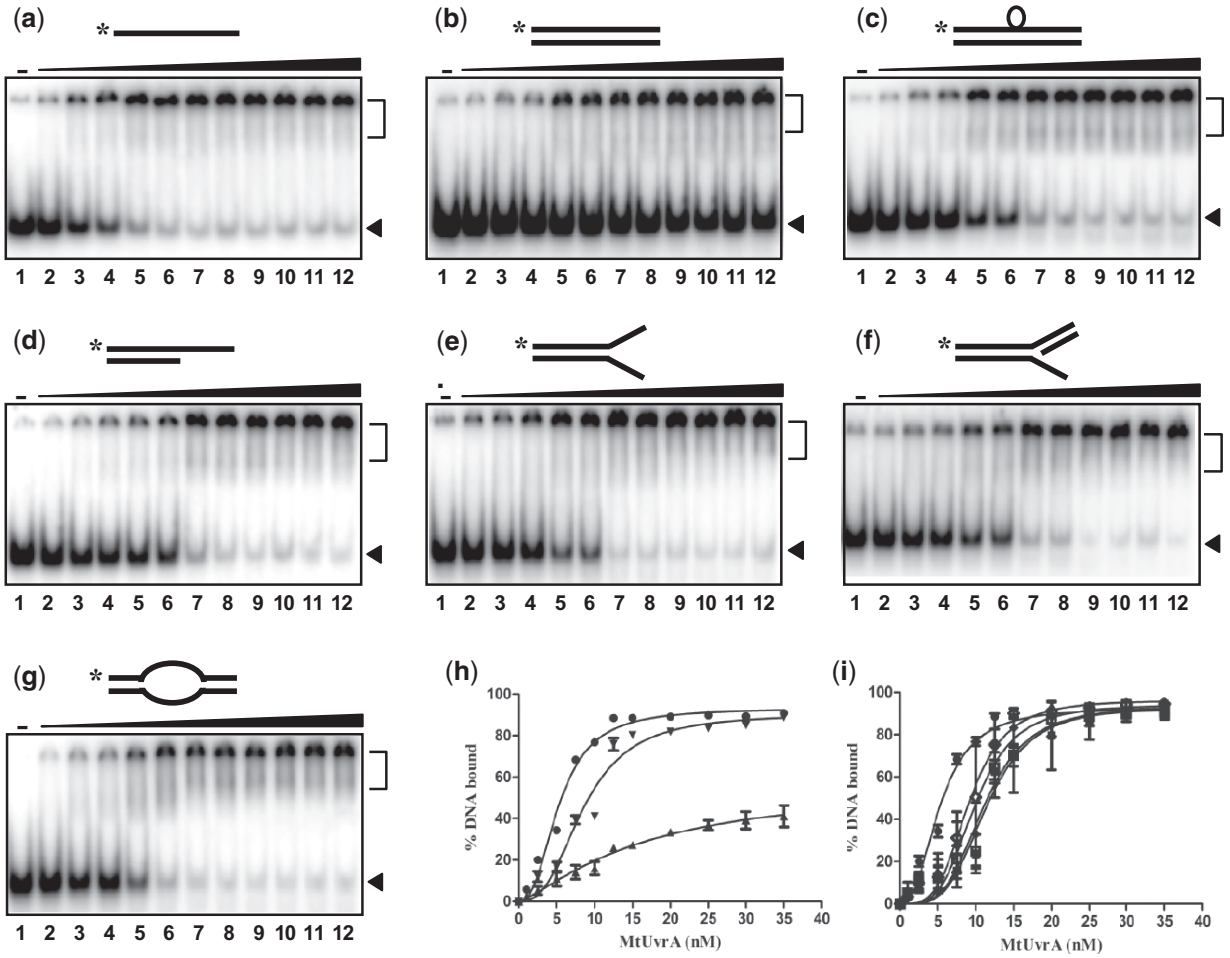


**Figure 2.** *Mycobacterium tuberculosis* UvrA binds preferentially to DNA intermediates containing single-stranded region. Reactions mixtures contained 250 pM of the indicated $^{32}$P-labelled substrate in the absence (lane 1) or presence of 1, 2.5, 5, 7.5, 10, 12.5, 15, 20, 25, 30 or 35 nM *Mt*UvrA (lanes 2–12), respectively. The filled triangle on top of each gel image represents increasing concentrations of *Mt*UvrA; in **a** to **g** panels the black arrowhead points to free-DNA and the squared bracket indicates *Mt*UvrA–DNA complexes. Panels: a, single-stranded DNA (ODN1); b, non-damaged duplex DNA (ODN1 annealed to ODN6); c, damaged duplex DNA (ODN7 annealed to ODN8); d, 5′-overhang (ODN1 annealed to ODN5); e, flayed duplex DNA (ODN1 annealed to ODN4); f, 5′-flap (ODN1, ODN4 annealed to ODN5); g, bubble duplex (ODN2 annealed to ODN3) (for ODNs sequence see Supplementary Table S1). In panel h, the percentage of *Mt*UvrA–DNA complex formation in panels a–c is plotted against the indicated amounts *Mt*UvrA. In panel i, the percentage of *Mt*UvrA–DNA complex formation in panel a and panels d to g is plotted against the indicated amounts *Mt*UvrA. (filled circle), *Mt*UvrA-single-stranded DNA; (filled square), *Mt*UvrA-5′-overhang; (filled diamond), *Mt*UvrA-flayed duplex DNA; (open square), *Mt*UvrA-5′-flap; (open diamond), *Mt*UvrA-bubble duplex DNA; (filled triangle), *Mt*UvrA-non-damaged duplex DNA; (filled inverted triangle), *Mt*UvrA-damaged duplex DNA. Each point on the curves represents the mean of three separate experiments. The best-fit curve was obtained by subjecting the data sets to non-linear regression analysis, in GraphPad PRISM (ver5.00), using the equation for one site specific binding with Hill slope.

believed to drive UvrA dimer dissociation and consequently reduces DNA binding (5). Despite this general picture, the mechanistic details of how ATP binding and its hydrolysis regulate the interaction of UvrA with DNA are poorly understood.

We used recombinant *Mt*UvrA to test the effect of single- and double-stranded DNA on its ATPase activity. Notably, we observed that *Mt*UvrA has a low intrinsic ATPase activity that can be stimulated by single- as well double-stranded DNA (Figure 3, panels a–c). Furthermore, stimulation was greater in the presence of double-stranded DNA compared to single-stranded DNA. In particular, we observed a 5-fold increase in ATPase activity in the presence of double-stranded DNA (Figure 3d). We conclude that the ATPase activity of *Mt*UvrA is more efficient in the presence of DNA than in its absence. Similarly, others have shown that the ATPase activity of *Bacillus caldotenax* UvrA was stimulated ~3-fold in the presence of single-stranded or damaged DNA (43).

### *Mt*UvrA overall structure

The structure of a ligand-free form of *Mt*UvrA was solved at 3.4 Å. Four out of the six chains that are present in the *Mt*UvrA asymmetric unit are arranged in two tight homodimers (namely BD and CE) showing the same quaternary structure arrangement described in the crystal structure of UvrA proteins reported so far (16–18), while the remaining A and F subunits are observed as independent monomers (Supplementary Figure S3, left panel).

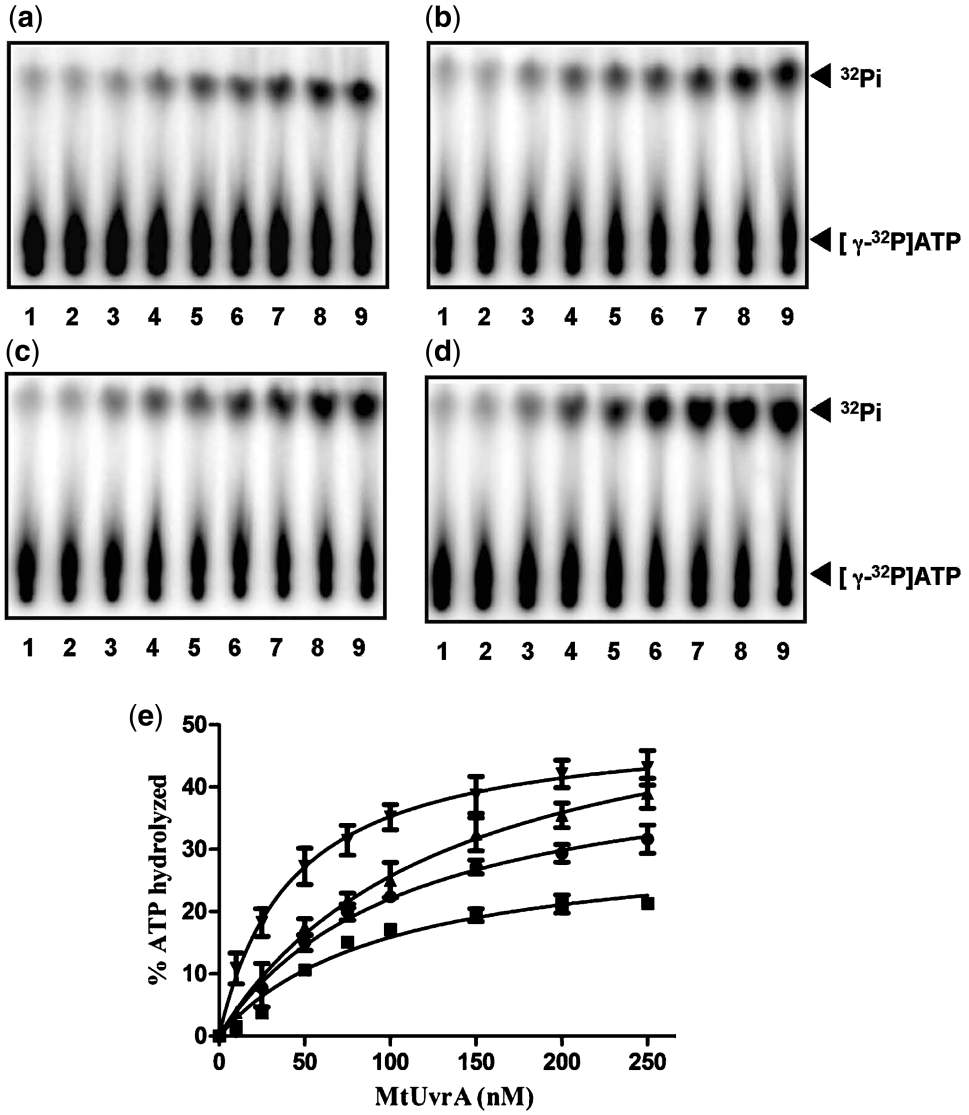


**Figure 3.** *Mycobacterium tuberculosis* UvrA is a DNA-dependent ATPase. Reactions mixtures contained 100 nM of the indicated DNA co-factor, 50 μM [γ-$^{32}$P]ATP in the absence (lane 1) or presence of 10, 25, 50, 75, 100, 150, 200 and 250 nM *Mt*UvrA (lanes 2–9), respectively. Panels: (**a**), *Mt*UvrA alone; (**b**), *Mt*UvrA in the presence of single-stranded DNA (ODN8); (**c**) *Mt*UvrA in the presence of non-damaged duplex DNA (ODN1 annealed to ODN6); (**d**) *Mt*UvrA in presence of damaged duplex DNA (ODN7 annealed to ODN8) (ODN sequences are listed in Supplementary Table S1). The positions of [γ-$^{32}$P]ATP and $^{32}$Pi is indicated on the right-hand side. Panel (**e**): graphical representation of ATPase activity of *Mt*UvrA as a function of protein concentration. The percentage of [γ-$^{32}$P]ATP hydrolyzed, in panels a–d, is plotted against the indicated amounts of *Mt*UvrA. (filled square), *Mt*UvrA in absence of DNA; (filled circle), *Mt*UvrA in the presence of single-stranded DNA; (filled triangle), *Mt*UvrA in the presence of non-damaged duplex DNA; (inverted filled triangle), *Mt*UvrA in the presence of damaged duplex DNA. Each point on the curves represents the mean of three separate experiments. Non-linear regression analysis (Michaelis-Menten) was applied to the data sets, using GraphPad PRISM ver5.00, for obtaining the best-fit curve.

Since these last subunits form equivalent dimers with crystallographic symmetry-related mates, hexameric assemblies, based on three identical homodimers and reminiscent of asymmetric saddles, are observed in the crystal lattice (Supplementary Figure S3, right panel). In order to investigate the occurrence of hexamers in solution we carried out a biochemical investigation by means of gel-filtration chromatography and atomic force microscopy (AFM). Size-exclusion chromatography revealed the presence of oligomeric assemblies sensibly larger than hexamers ('Materials and Methods' section in Supplementary Data and Supplementary Figure S2b). On the other hand, when inspected by AFM in water environment ('Material and Methods' and 'Results' in Supplementary Data) *Mt*UvrA displayed the typical pattern shown in the Supplementary Figure S4, where globular objects of homogeneous size corresponding to dimers, represented the prevailing morphology. We, therefore, conclude that the oligomeric assembly observed in the crystal is unlikely to have a physiological significance and appears more likely the result of experimental conditions (i.e. crystal lattice constrains and/or high protein

concentration). Instead, a classic dimeric organization emerges as the functional unit in *Mt*UvrA as described in other species.

Similarly to what has been observed in the structures of UvrAs reported so far (16–18)—independently from their membership to class I or class II, the molecular architecture of each *Mt*UvrA chain (Figure 4a) is organized around a roughly globular catalytic core split in two NBD (NBD-I and NBD-II) that contribute to build up two functional ATP/ADP binding sites by juxtaposition

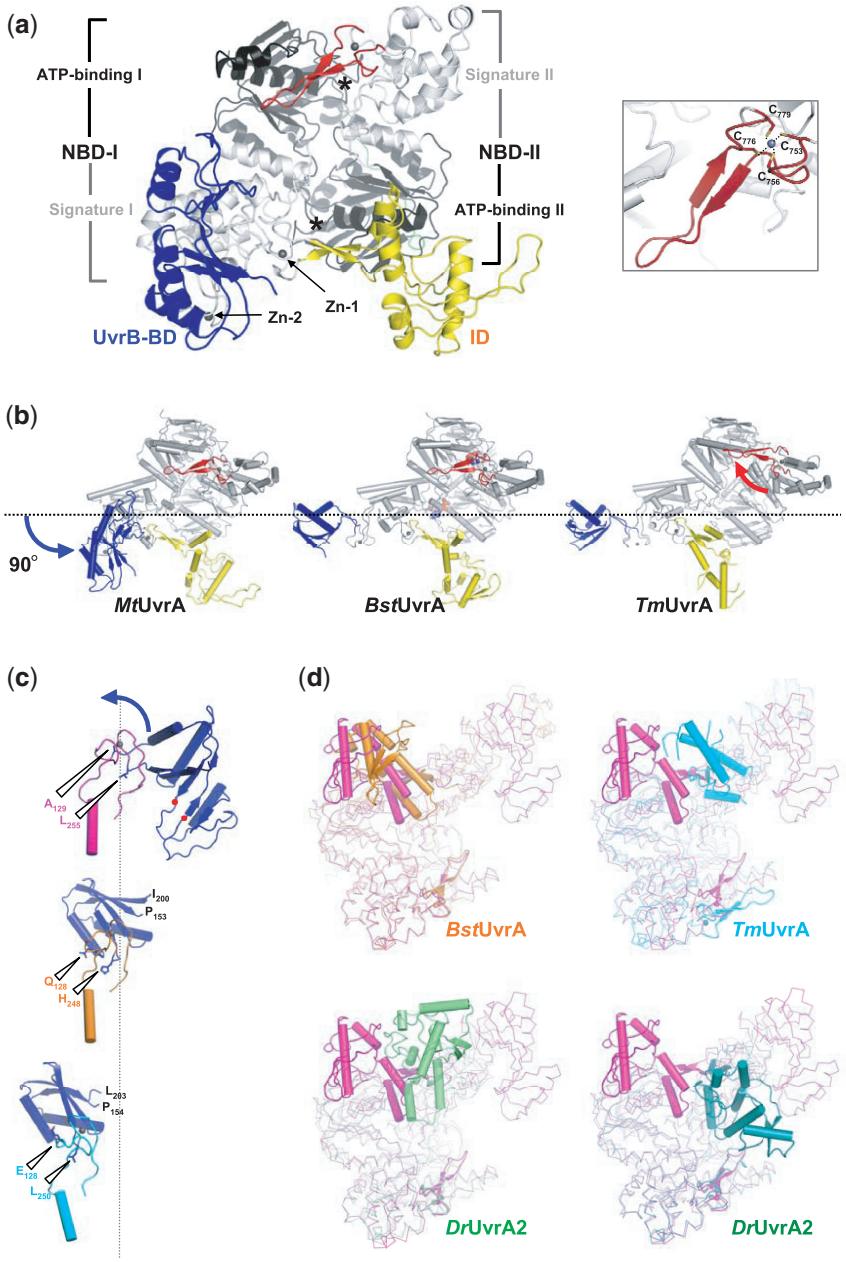


**Figure 4.** *Mt*UvrA molecular architecture. (**a**) Cartoon representation of a *Mt*UvrA subunit; the C-terminal Zn finger and the NBDs-connecting loop are depicted in red and green, respectively; the asterisks label the position of the nucleotide binding sites; a close-up view of the C-terminal Zn finger appears in the inset, where the $Zn^{++}$ ion and the four metal coordinating cysteine residues are drawn as a black sphere and sticks, respectively; the $Zn^{++}$ coordinative bonds, involving Cys753 (2.3 Å), Cys756 (2.4 Å), Cys776 (2.4 Å) and Cys779 (2.4 Å), are indicated by dotted lines. The UvrB binding domain (UvrB-BD) and the insertion domain (ID) are coloured blue and yellow, respectively and the two Zn modules are indicated. (**b**) Cartoon representation of *Mt*UvrA (left; PDB code 2ygr), *Bst*UvrA (middle; PDB code 2R6F) and *Tm*UvrA (right; PDB code 3PIH) monomers upon optimal superposition; the direction of the rotation of the UvrB-BD is indicated by the blue arrow; the red arrow highlights the displacement of the C-terminal Zn finger observed in *Tm*UvrA upon modified DNA binding (the DNA molecule has been omitted). (**c**) Close-up views of the flexible region located between the Zn module 1 and the UvrB-BD in *Mt*UvrA (top), *Bst*UvrA (middle) and *Tm*UvrA (bottom), upon optimal superposition; the arrows point to structurally equivalent residues in the structures in order to focusing the pivotal region for the observed domain rotation. The red spots label the borders of the 155–200 region of *Mt*UvrA UvrB-BD that is disordered in both the *Bst*UvrA and *Tm*UvrA crystal structures (corresponding delimiting residues are indicated). (**d**) Ribbon representation of the indicated UvrA monomer optimally superimposed to the *Mt*UvrA structure (magenta); the ID domain in each structure has been rendered as cartoon to highlight its conformational flexibility.

and that are connected by a conserved flexible loop (residues 608–625). The comparison of the catalytic core of *Mt*UvrA with the equivalent region of available UvrA structures revealed no significant conformational changes, allowing us to affirm that the bulk body of UvrA is highly structurally conserved in different species. At the same time, our data add an independent confirmation to the emerging concept that the structuring of the ATP/ADP binding sites of each UvrA monomer depends exclusively on the observed intra-chain folding and not on oligomerization events.

In parallel to what revealed by the crystal structure of *Bacillus stearothermophilus* (16) and *T. maritima* (17) UvrA, the NBD-I of *Mt*UvrA appears to be interrupted by an additional 'dumb-bell'-folded region, distinguishing these proteins from other ABC ATPase superfamily members (15); in class I UvrAs this peculiar region consists of the UvrB binding domain (UvrB-BD, residues 129–255) and of the insertion domain (ID, residues 290–411), which are jointed by a stem bearing the Zn modules 1 and 2 (Figure 4a). Finally, the DNA recognizing C-terminal Zn finger (residues 753–779), which buds from the NBD-II and points towards the interior of the monomer, contains a zinc ion that coordinates four strictly conserved cysteine residues with tetrahedral geometry (Figure 4a, inset).

Previous studies suggested that the UvrB-BD could be subjected to major movements in order to deliver bound UvrB protein to the damaged DNA molecule (16,17,21), which is indeed housed at the ventral surface of the UvrA functional dimer upon the displacement of the C-terminal Zn fingers (17). Similarly, the structural comparison of *Dr*UvrA2 protomers in different ligand-bound states showed the ability of the ID to undergo dramatic repositioning during DNA recognition and nucleotide binding (18).

Interestingly, the optimal superposition of the structure of ligand-free *Mt*UvrA to either *Bst*UvrA in complex with ADP (16) or *Tm*UvrA associated with damaged DNA (17) (r.m.s.d. of 1.2 and 3.9 Å for the 582 Cα pairs building up the catalytic domain, respectively) as well as to DrUvrA2 (r.m.s.d. ranging from 1.8 to 2.0 Å for 503 Cα pairs, depending on the chain and the model considered) revealed a remarkable structural rearrangement affecting the UvrB-BD and ID domains. In particular, in *MtUvrA* the UvrB-BD appears to undergo a striking 90° rotation towards the interior of the protein compared to the conformation it assumes in the other two class I UvrA structural models, where it is observed as fully exposed to the bulk solvent (Figure 4b and c, Supplementary Movie 1). Moreover, the ID in *Mt*UvrA adopts the most open conformation with respect to what observed in the structures of *Bst*UvrA•ADP and *Tm*UvrA•DNA as well as *Dr*UvrA2 in which it is located closer to the central axis of the monomer (Figure 4d).

Overall our observation further highlights the conformational flexibility featuring the UvrB-BD and ID in UvrA proteins and strongly supports the view that significant conformational changes, possibly triggered by substrates binding, accompany the dynamics of the functional interplay between UvrA, UvrB and the DNA (19).

### Structural analysis of the *Mt*UvrA functional dimer

The peculiar conformation adopted by the UvrB-BD in ligand-free *Mt*UvrA profoundly impacts the overall architecture of the functional homodimer, compared to the structure of UvrA in complex either with ADP (16) or modified dsDNA (17) (Figure 5). Indeed, while a number of molecular contacts, involving residues of the dorsal side of opposing subunits, are conserved in UvrA structures reported so far, including *Dr*UvrA2 (Supplementary Figure S5), in the *Mt*UvrA structure additional inter-chain bonds are established between the region Lys160–Asp165 of the UvrB-BD of one subunit and residues adjacent to the C-terminal Zn finger of the opposing monomer in the dimer (Figure 5, inset). It must be noticed that in both *Bst*UvrA•ADP and *Tm*UvrA•DNA structures the equivalent region of UvrB-BD is disordered (Figures 4 and 5), most probably due to the fact that it is not stabilized by protein–protein contacts as it is in *Mt*UvrA.

Based upon molecular modelling (Figure 6a) the distinctive arrangement displayed by the *Mt*UvrA dimer would not hamper the accessibility of ideal double-stranded DNA to the highly conserved residues Arg725, Lys735, Arg737 and Arg743, whose structural equivalents have been demonstrated to be essential for DNA binding in *Bst*UvrA by site-directed mutagenesis (16). In contrast, when we modelled the modified DNA molecule as observed in *Tm*UvrA•DNA structure (17) in the optimally superimposed *Mt*UvrA dimer, steric hindrance became appreciable on both sides of the fluoresceinated-dT containing lesion at the level of both the UvrB-BD and the C-terminal Zn fingers (Figure 6b and Supplementary Movie).

### Modelling of the UvrA•UvrB complex in different states

When we superimposed the UvrB-BD of *Mt*UvrA onto the crystal structure of *B. stearothermophilus* UvrA•UvrB complex, which consists only of the reciprocally interacting domains of the two partners (21), no major structural rearrangements could be observed and the conformation adopted by the UvrB-BD domain in our ligand-free *Mt*UvrA structure appears to be accessible by UvrB (Figure 7a). Therefore, based on such a structural superposition, we constructed a model of the *Mt*UvrA•UvrB complex (Figure 8b, left panel) by using the crystal structure of full-length UvrB from *B. caldotenax* in complex with a 20 bp haipin DNA substrate containing a fluoresceinated-dT adduct (PDB-ID: 2FDC) (46). The resulting *Mt*UvrA•UvrB complex would be compatible with both an $UvrA_2$•$UvrB_2$ (Figure 7b, upper panels) and an $UvrA_2$•UvrB (not shown) stoichiometry. Moreover, the different conformation adopted by the UvrB-BD, respectively, in the structure of ligand-free *Mt*UvrA, *Bst*UvrA•ADP (16) and *Tm*UvrA•DNA (17) (Figure 7b, from top to bottom), appears in all cases competent for the concomitant association to UvrB and DNA, although with different geometry. In fact, while in the *Mt*$UvrA_2$•$UvrB_2$ model the double-strand DNA should be hosted inside an only partially solvent-accessible track, which is built up by the facing ventral surfaces of

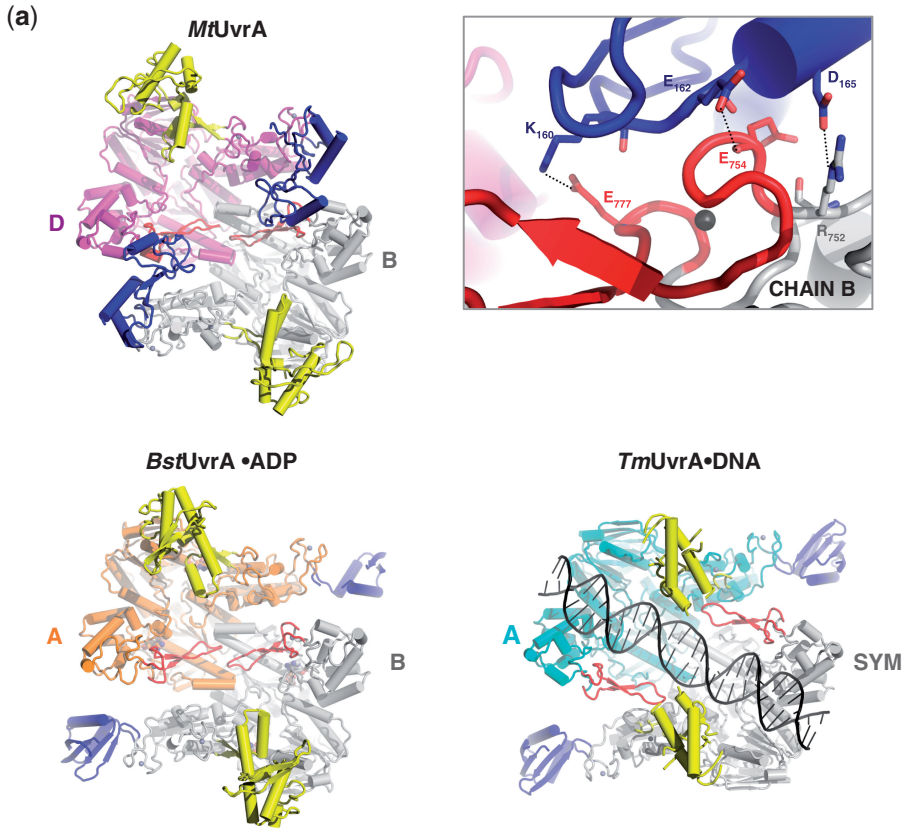


**Figure 5.** *Mt*UvrA dimer organization. (**a**) Comparison between the functional dimeric assemblies of *Mt*UvrA (upper side, left), *Bst*UvrA (lower side, left) and *Tm*UvrA (lower side, right) as viewed from their ventral surface, upon optimal superposition; the two catalytic cores in each dimer are coloured magenta and white in *Mt*UvrA, orange and white in *Bst*UvrA and cyan and white in *Tm*UvrA; the UvrB-BD, the ID and the C-terminal Zn finger are invariably coloured blue, yellow and red, respectively; DNA appears in black. The inset depicts a close-up view of the peculiar interactions observed in the *Mt*UvrA dimer on its ventral side; residues participating in main stabilizing contacts are shown as sticks.

both protein components, in the other two models the UvrB-BD repositioning would result in the exposure of the DNA molecule to the bulk solvent. We therefore propose that the described three alternative conformations could represent different structural snapshots along the process of UvrB delivering to the damaged DNA.

On the basis of the available structural information, we are tempted to propose the following model, possibly illustrating the sequence of the first steps in NER (Figure 8). According to this model, the $UvrA_2$•$UvrB_2$ structural unit scanning DNA could display the UvrB-BDs in the closed conformation we observe in the structure of the ligand-free MtUvrA. Upon ATP hydrolysis taking place in UvrA the UvrB-BDs would flip out resulting in the conformation observed in *Bst*UvrA•ADP (16); however, this would be insufficient to promote both $UvrA_2$•$UvrB_2$ complex disassembling and $UvrA_2$ dimer dissociation. When a lesion is encountered on DNA, the displacement of the UvrB-BDs could unlock the C-terminal Zn fingers that could move apart one from each other to make room for the DNA molecule;

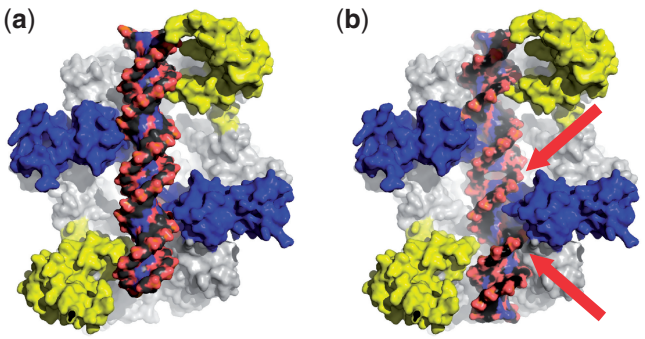


**Figure 6.** Modelling of double-strand DNA binding within the *Mt*UvrA dimer. The image in (**a**) shows the manual best fitting of an ideal form-B DNA molecule (28 bp) onto the ventral surface of the *Mt*UvrA dimer; the image in (**b**) shows the position occupied within the *Mt*UvrA dimer by the modified DNA as observed in *Tm*UvrA•DNA crystal structure (PDB code 3PIH) upon optimal superposition of the two structures; the red arrows point to the molecular clashes observed between the modified DNA backbone and the protein environment. In both pictures the UvrB-BD, the ID and the C-terminal Zn finger of both monomers are coloured blue, yellow and red, respectively.

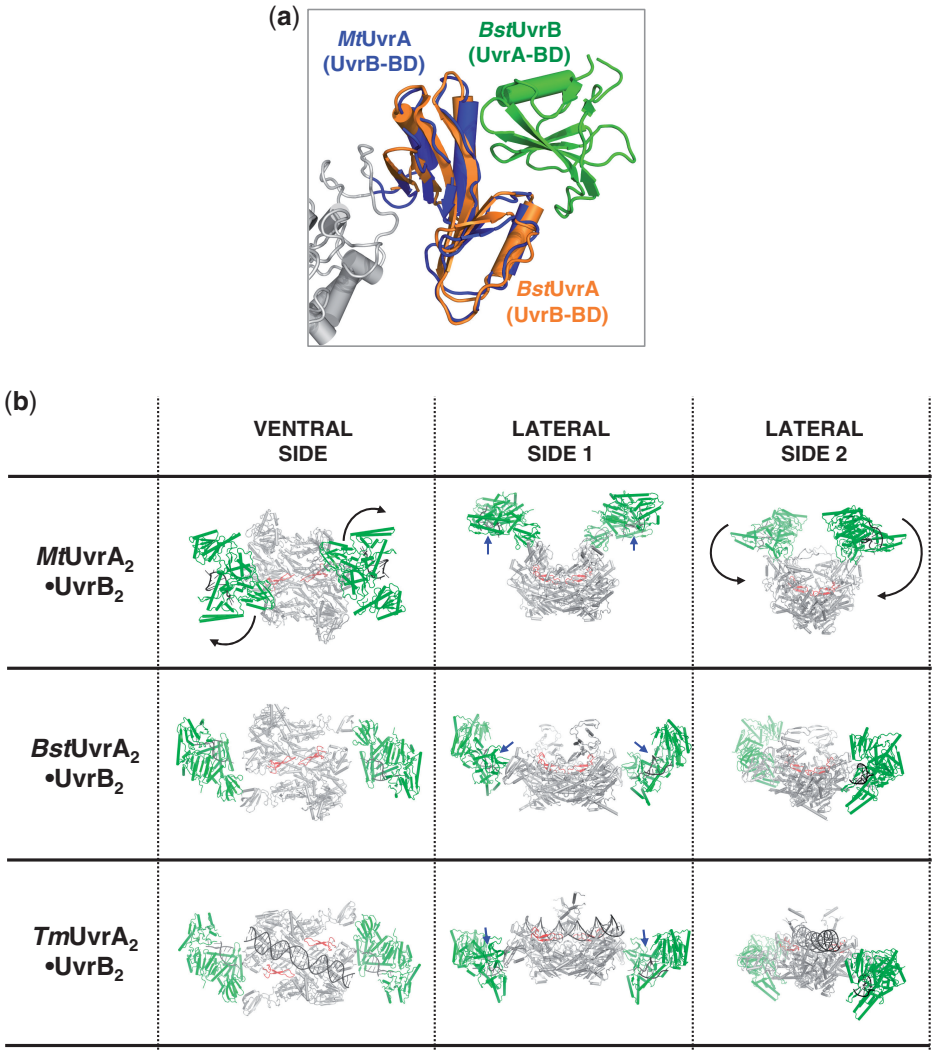


**Figure 7.** Modelling of the association of UvrA to UvrB. (**a**) Cartoon representation of *B. stearothermophilus* UvrA•UvrB complex (PDB code 3FPN) and *Mt*UvrA upon optimal structural superposition (r.m.s.d. deviation of 1.8 Å based on 107 Cα pairs belonging to UvrB-BD); the UvrA binding domain (UvrA-BD) of *Bst*UvrB appears in green, while the superposed UvrB-BDs of *Bst*UvrA and *Mt*UvrA are coloured orange and blue, respectively. (**b**) Cartoon representations of $UvrA_2$•$UvrB_2$ complex models as obtained by optimal superposition of the *Bacillus caldotenax* UvrB structure (PDB code 2FDC) onto the *B. stearothermophilus* UvrA•UvrB complex superposed to *M. tuberculosis* (top images), *B. stearothermophilus* (middle images) and *T. maritima* (bottom images) UvrA crystal structures (three alternative points of view are shown). In all images UvrB is uniformly coloured green, while the C-terminal Zn fingers in each UvrA dimer and DNA molecules appear in red and black, respectively; the black arrows indicate the direction of the displacement of the UvrB-BDs of *Mt*UvrA; the blue arrows point toward the ventral surface of the UvrB chains.

this phenomenon indeed observed in the *Tm*UvrA•DNA crystal structure (17) weakens the inter-chain contacts stabilizing the $UvrA_2$ dimer, which could subsequently dissociate leaving UvrB bound to the damaged DNA.

## CONCLUSIONS

NER is an extremely conserved molecular system that governs DNA integrity and stability in all organisms (4); however, the proteins acting in the first events of this pathway substantially differ between bacteria and eukaryotic cells (37) and bioinformatics analyses fail in identifying human orthologues of the UvrABC components. Our results provide experimental evidence that UvrA is required for optimal *M. tuberculosis* survival to physiological DNA-damaging stress, possibly implicating this gene in the persistence of the bacillus in the host. The herein reported crystal structure of UvrA in its ligand-free form further highlights the remarkable conformational plasticity displayed by UvrA along the series of molecular events that features the protein function. Overall, our genetics, biochemical and structural investigations revealed novel insights into the function of *Mt*UvrA and provide a significant contribution toward the understanding of the mechanistic aspects of the NER pathway in *M. tuberculosis*.

## ACCESSION NUMBER

The atomic coordinates and structure factors have been deposited with the Protein Data Bank with the accession code 2ygr.

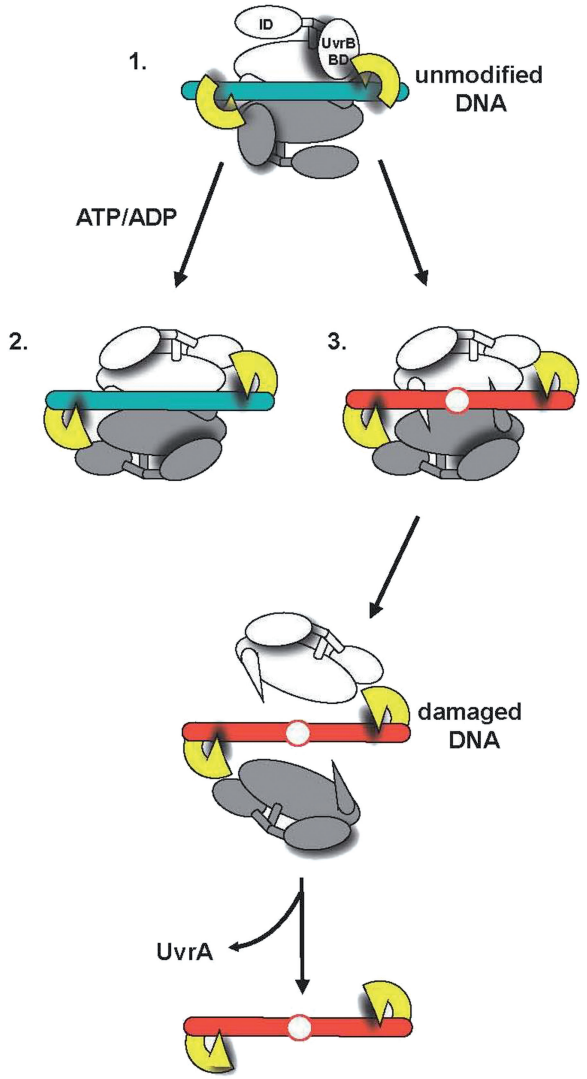


**Figure 8.** Structure-based model of possible UvrA/UvrB/DNA interactions. The UvrA dimer is in principle capable simultaneous interaction with both UvrB (depicted in yellow) and the DNA substrate in all the alternative conformations disclosed by structural studies [(1) Ligand-free, (2) ADP-bound and (3) in complex to modified DNA]; however, in the presence of distorted damaged DNA that causes a weakening of UvrA inter-subunit contacts, UvrA dissociation would occur leaving UvrB stably associated to the DNA.

## SUPPLEMENTARY DATA

Supplementary Data are available at NAR Online.

## ACKNOWLEDGEMENTS

We acknowledge the European Synchrotron Radiation Facility for provision of synchrotron radiation facilities and we would like to thank Dr. Martin Walsh for assistance in using BM14 UK beamline. We would like to thank Heran Darwin and Carl Nathan (New York University School of Medicine, USA) for kindly providing us with the *M. tuberculosis uvrB* mutant strain.

## FUNDING

Funding for open access charge: European Community (projects CSI_LTB LSHPCT-2007-037235 and SysteMTb HEALTH-F4-2010-241587); UK Medical Research Council (programme number U1175 32056).

*Conflict of interest statement*. None declared.

## REFERENCES

1. Dos Vultos,T., Mestre,O., Tonjum,T. and Gicquel,B. (2009) DNA repair in *Mycobacterium tuberculosis* revisited. *FEMS Microbiol. Rev.*, **33**, 471–487.
2. Mizrahi,V. and Andersen,S.J. (1998) DNA repair in *Mycobacterium tuberculosis*. What have we learnt from the genome sequence? *Mol. Microbiol.*, **29**, 1331–1339.
3. Warner,D.F. and Mizrahi,V. (2007) The survival kit of *Mycobacterium tuberculosis*. *Nat. Med.*, **13**, 282–284.
4. Petit,C. and Sancar,A. (1999) Nucleotide excision repair: from E. coli to man. *Biochimie*, **81**, 15–25.
5. Truglio,J.J., Croteau,D.L., Van Houten,B. and Kisker,C. (2006) Prokaryotic nucleotide excision repair: the UvrABC system. *Chem. Rev.*, **106**, 233–252.
6. Van Houten,B. (1990) Nucleotide excision repair in *Escherichia coli*. *Microbiol. Rev.*, **54**, 18–51.
7. Goosen,N. and Moolenaar,G.F. (2008) Repair of UV damage in bacteria. *DNA Repair*, **7**, 353–379.
8. Malta,E., Moolenaar,G.F. and Goosen,N. (2007) Dynamics of the UvrABC nucleotide excision repair proteins analyzed by fluorescence resonance energy transfer. *Biochemistry*, **46**, 9080–9088.
9. Kad,N.M., Wang,H., Kennedy,G.G., Warshaw,D.M. and Van Houten,B. (2010) Collaborative dynamic DNA scanning by nucleotide excision repair proteins investigated by single-molecule imaging of quantum-dot-labeled proteins. *Mol. Cell*, **37**, 702–713.
10. Graham,J.E. and Clark-Curtiss,J.E. (1999) Identification of *Mycobacterium tuberculosis* RNAs synthesized in response to phagocytosis by human macrophages by selective capture of transcribed sequences (SCOTS). *Proc. Natl Acad. Sci. USA*, **96**, 11554–11559.
11. Darwin,K.H., Ehrt,S., Gutierrez-Ramos,J.C., Weich,N. and Nathan,C.F. (2003) The proteasome of *Mycobacterium tuberculosis* is required for resistance to nitric oxide. *Science*, **302**, 1963–1966.
12. Darwin,K.H. and Nathan,C.F. (2005) Role for nucleotide excision repair in virulence of *Mycobacterium tuberculosis*. *Infect. Immun.*, **73**, 4581–4587.
13. Kurthkoti,K., Kumar,P., Jain,R. and Varshney,U. (2008) Important role of the nucleotide excision repair pathway in *Mycobacterium smegmatis* in conferring protection against commonly encountered DNA-damaging agents. *Microbiology*, **154**, 2776–2785.
14. Mazloum,N., Stegman,M.A., Croteau,D.L., Van Houten,B., Kwon,N.S., Lin,Y., Dickinson,C., Venugopal,A., Towheed,M.A. and Nathan,C. (2011) Identification of a chemical that inhibits the mycobacterial UvrABC complex in nucleotide excision repair. *Biochemistry*, **50**, 1329–1335.
15. Davidson,A.L., Dassa,E., Orelle,C. and Chen,J. (2008) Structure, function, and evolution of bacterial ATP-binding cassette systems. *Microbiol. Mol. Biol. Rev.*, **72**, 317–364.
16. Pakotiprapha,D., Inuzuka,Y., Bowman,B.R., Moolenaar,G.F., Goosen,N., Jeruzalmi,D. and Verdine,G.L. (2008) Crystal structure of *Bacillus stearothermophilus* UvrA provides insight into ATP-modulated dimerization, UvrB interaction, and DNA binding. *Mol. Cell*, **29**, 122–133.
17. Jaciuk,M., Nowak,E., Skowronek,K., Tańska,A. and Nowotny,M. (2011) Structure of UvrA nucleotide excision repair protein in complex with modified DNA. *Nat. Struct. Mol. Biol.*, **18**, 191–197.
18. Timmins,J., Gordon,E., Caria,S., Leonard,G., Acajjaoui,S., Kuo,M.S., Monchois,V. and McSweeney,S. (2009) Structural and

mutational analyses of *Deinococcus radiodurans* UvrA2 provide insight into DNA binding and damage recognition by UvrAs. *Structure*, **17**, 547–558.
19. Goosen,N. and Moolenaar,G.F. (2001) Role of ATP hydrolysis by UvrA and UvrB during nucleotide excision repair. *Res. Microbiol.*, **152**, 401–409.
20. Wagner,K., Moolenaar,G., van Noort,J. and Goosen,N. (2009) Single-molecule analysis reveals two separate DNA-binding domains in the *Escherichia coli* UvrA dimer. *Nucleic Acids Res.*, **37**, 1962–1972.
21. Pakotiprapha,D., Liu,Y., Verdine,G.L. and Jeruzalmi,D. (2009) A structural model for the damage-sensing complex in bacterial nucleotide excision repair. *J. Biol. Chem.*, **284**, 12837–12844.
22. Croteau,D.L., DellaVecchia,M.J., Perera,L. and Van Houten,B. (2008) Cooperative damage recognition by UvrA and UvrB: identification of UvrA residues that mediate DNA binding. *DNA Repair*, **7**, 392–404.
23. Davis,E.O., Springer,B., Gopaul,K.K., Papavinasasundaram,K.G., Sander,P. and Bottger,E.C. (2002) DNA damage induction of *recA* in *Mycobacterium tuberculosis* independently of RecA and LexA. *Mol. Microbiol.*, **46**, 791–800.
24. Sander,P., Meier,A. and Bottger,E.C. (1995) rpsL+: a dominant selectable marker for gene replacement in mycobacteria. *Mol. Microbiol.*, **16**, 991–1000.
25. Brosch,R., Gordon,S.V., Billault,A., Garnier,T., Eiglmeier,K., Soravito,C., Barrell,B.G. and Cole,S.T. (1998) Use of a *Mycobacterium tuberculosis* H37Rv bacterial artificial chromosome library for genome mapping, sequencing, and comparative genomics. *Infect. Immun.*, **66**, 2221–2229.
26. Rickman,L., Saldanha,J.W., Hunt,D.M., Hoar,D.N., Colston,M.J., Millar,J.B. and Buxton,R.S. (2004) A two-component signal transduction system with a PAS domain-containing sensor is required for virulence of *Mycobacterium tuberculosis* in mice. *Biochem. Biophys. Res. Commun.*, **314**, 259–267.
27. Springer,B., Sander,P., Sedlacek,L., Ellrott,K. and Bottger,E.C. (2001) Instability and site-specific excision of integration-proficient mycobacteriophage L5 plasmids: development of stably maintained integrative vectors. *Int. J. Med. Microbiol.*, **290**, 669–675.
28. Sambrook,J., Fritsh,E.F. and Maniatis,T. (1989) *Molecular Cloning: A Laboratory Manual*, 2nd edn. Cold Spring Harbor Laboratory Press, Cold Spring Harbor, NY.
29. Tripathi,P., Anuradha,S., Ghosal,G. and Muniyappa,K. (2006) Selective binding of meiosis-specific yeast Hop1 protein to the holliday junctions distorts the DNA structure and its implications for junction migration and resolution. *J. Mol. Biol.*, **364**, 599–611.
30. Collaborative Computational Project, Number 4 (CCP4). (1994) The CCP4 suite: programs for protein crystallography. *Acta Crystallogr. D Biol. Crystallogr.*, **50**, 760–763.
31. McCoy,A.J., Grosse-Kunstleve,R.W., Adams,P.D., Winn,M.D., Storoni,L.C. and Read,R.J. (2007) Phaser crystallographic software. *J. Appl. Crystallogr.*, **40**, 658–674.
32. Cowtan,K. and Main,P. (1998) Miscellaneous algorithms for density modification. *Acta Crystallog. D Biol. Crystallogr.*, **54**, 487–493.
33. Adams,P.D., Afonine,P.V., Bunkóczi,G., Chen,V.B., Davis,I.W., Echols,N., Headd,J.J., Hung,L.-W., Kapral,G.J., Grosse-Kunstleve,R.W. *et al.* (2010) PHENIX: a comprehensive Pythonbased system for macromolecular structure solution. *Acta Crystallogr. D Biol. Crystallogr.*, **66**, 213–221.
34. Emsley,P. and Cowtan,K. (2004) Coot: model-building tools for molecular graphics. *Acta Crystallogr. D Biol. Crystallogr.*, **60**, 2126–2132.
35. Laskowski,R.A., MacArthur,M.W., Moss,D.S. and Thornton,J.M. (1993) PROCHECK: a program to check the stereochemical quality of protein structures. *J. Appl. Crystallogr.*, **26**, 283–291.
36. DeLano,W.L. (2002) *The PyMOL Molecular Graphics System*. DeLano Scientific, Palo Alto, CA, USA.
37. Friedberg,E.C., Walker,G.C. and Siede,W. (1995) *DNA Repair and Mutagenesis*. American Society for Microbiology Press, Washington, DC.
38. Iyer,V.N. and Szybalski,W. (1963) A molecular mechanism of mitomycin action: Linking of complementary DNA strands. *Proc. Natl Acad. Sci. USA*, **50**, 355–362.
39. Tomasz,M., Lipman,R., Chowdary,D., Pawlak,J., Verdine,G.L. and Nakanishi,K. (1987) Isolation and structure of a covalent cross-link adduct between mitomycin C and DNA. *Science*, **235**, 1204–1208.
40. Burney,S., Caulfield,J.L., Niles,J.C., Wishnok,J.S. and Tannenbaum,S.R. (1999) The chemistry of DNA damage from nitric oxide and peroxynitrite. *Mutat. Res.*, **424**, 37–49.
41. Mahler,H.C., Schulz,I., Adam,W., Grimm,G.N., Saha-Moller,C.R. and Epe,B. (2001) *tert*-Butoxyl radicals generate mainly 7,8-dihydro-8-oxoguanine in DNA. *Mutat. Res.*, **461**, 289–299.
42. Hix,S., Morais Mda,S. and Augusto,O. (1995) DNA methylation by tert-butyl hydroperoxide-iron (II). *Free Radic. Biol. Med.*, **19**, 293–301.
43. Croteau,D.L., DellaVecchia,M.J., Wang,H., Bienstock,R.J., Melton,M.A. and Van Houten,B. (2006) The C-terminal zinc finger of UvrA does not bind DNA directly but regulates damage-specific DNA binding. *J. Biol. Chem.*, **281**, 26370–26381.
44. Seeberg,E. and Steinum,A.L. (1982) Purification and properties of the uvrA protein from *Escherichia coli*. *Proc. Natl Acad. Sci. USA*, **79**, 988–992.
45. Oh,E.Y., Claassen,L., Thiagalingam,S., Mazur,S. and Grossman,L. (1989) ATPase activity of the UvrA and UvrAB protein complexes of the *Escherichia coli* UvrABC endonuclease. *Nucleic Acids Res.*, **17**, 4145–4159.
46. Truglio,J.J., Karakas,E., Rhau,B., Wang,H., DellaVecchia,M.J., Van Houten,B. and Kisker,C. (2006) Structural basis for DNA recognition and processing by UvrB. *Nat. Struct. Mol. Biol.*, **13**, 360–364.